Cerebral Cortex October 2015;25:3458–3467
doi:10.1093/cercor/bhu169
Advance Access publication August 6, 2014

Imprecise Whisker Map in the Neonatal Rat Barrel Cortex

Olga Mitrukhina[1,2,3,†], Dmitry Suchkov[3,†], Roustem Khazipov[1,2,3] and Marat Minlebaev[1,2,3]

[1]INMED/INSERM U901, Marseille, France, [2]Aix-Marseille University, Marseille, France and [3]Laboratory of Neurobiology, Kazan Federal University, Kazan, Russia

Address correspondence to Roustem Khazipov, INMED/INSERM U901, 163 Avenue de Luminy, 13009 Marseille, France.
Email: roustem.khazipov@inserm.fr
[†]O.M. and D.S. contributed equally to this work.

The somatosensory barrel cortex in rodents contains a topographic map of the facial whiskers where each cortical barrel is tuned to a corresponding whisker. However, exactly when this correspondence is established during development and how precise the functional topography of the whisker protomap is at birth, before the anatomical formation of barrels, are questions that remain unresolved. Here, using extracellular and whole-cell recordings from the barrel cortex of 0- to 7-day-old (P0–7; P0 = day of birth) rat pups *in vivo*, we report a low level of tuning to the principal whisker at P0–1, with multiple adjacent whiskers evoking large multi- and single-unit responses and excitatory postsynaptic currents in cortical neurons. Additionally, we found broad and largely overlapping projection fields (PFs) for neighboring whiskers in the barrel cortex at P0–1. Starting from P2–3, a segregated whisker map emerged, characterized by preferential single whisker tuning and segregated whisker PFs. These results indicate that the functional whisker protomap in the somatosensory cortex is imprecise at birth, that for 2–3 days after birth, whiskers compete for the cortical target territories, and that formation of a segregated functional whisker map coincides with emergence of the anatomical barrel map.

Keywords: development, EEG patterns, electrophysiology, neonatal rat, somatosensory cortex

Introduction

The establishment of point-to-point sensory maps during development requires that afferent inputs restrict their connections to a limited number of selected target neurons (Rebsam et al. 2002). The dominant sequential developmental model involves 2 steps: (1) formation of initial basic "protomaps," where both the axon path and the primary connections are guided by molecular cues, and (2) refinement and elaboration of sensory maps through competition by the afferent inputs for their targets provided by spontaneous activity patterns and by early experience (Rakic 1976; Katz and Shatz 1996; Lopez-Bendito et al. 2003; O'Leary and Sahara 2008; Rakic et al. 2009; Erzurumlu and Gaspar 2012). However, whether cortical protomaps are precise from the start, and whether early activities support competitive interactions between the afferents, remains largely unknown.

To address this question, we examined the functional topography of the rat whisker-related somatosensory cortex during the early postnatal period. The primary somatosensory cortex in rodents contains a somatotopic map where each individual whisker is represented in a discrete cytoarchitectural L4 unit, the "barrel" (Woolsey and Van der Loos 1970; Petersen 2007; Fox 2008). Within each barrel, neurons are selectively tuned and respond with short-latency action potentials to stimulation of only 1 (principal) whisker (Simons 1978; Armstrong-James and Fox 1987; Brecht and Sakmann 2002; Roy et al. 2011). This selectivity is determined by topological organization of synaptic connections along a trisynaptic trigeminal lemniscal pathway involving trigeminal projections from a whisker to the corresponding barrelettes in the brainstem, from the barrelettes to barreloids in the VPM thalamus, and finally, from the barreloids to cortical barrels (Petersen 2007; Fox 2008). At the cortical level, selectivity of sensory information transfer from thalamus to cortex is ensured by segregation of thalamic axons, which branch primarily within the corresponding barrel, restricted to a barrel dendritic tree of the thalamorecipient L4 neurons, reach synaptic connectivity between excitatory L4 neurons within barrels, and surround inhibition (Feldmeyer et al. 2013).

During development, an anatomical barrel map forms during the first postnatal week, a critical period for barrel map plasticity. During this time, sensory deprivation or alteration in central activity results in dramatic changes to map organization, suggesting that sensory-driven activity plays a critical role in barrel map formation (Feldman and Brecht 2005; Fox 2008; Feldman 2009; Erzurumlu and Gaspar 2012). Previous studies on the barrel cortex revealed characteristic spontaneous and sensory-evoked bursting activity patterns during the postnatal period including delta waves, spindle bursts and early gamma oscillations (EGOs) (Armstrong-James 1975; McCandlish et al. 1993; Minlebaev et al. 2007; Minlebaev et al. 2009; Yang et al. 2009; Colonnese et al. 2010; Mohns and Blumberg 2010; Minlebaev et al. 2011; Yang et al. 2012; Tolner et al. 2012; Khazipov et al. 2013). During the first 2 postnatal days, sensory stimulation evokes electrical responses in the dense cortical plate, characterized by negative delta waves and spindle-burst oscillations associated with multiunit bursts. Starting from P2, EGOs are observed, and the typical response evoked by whisker stimulation consists of initial EGOs followed by spindle-burst oscillations until P7, when sensory responses switch from bursting to acuity (Colonnese et al. 2010; Minlebaev et al. 2011; Yang et al. 2012). Comparison of the multiunit and whole-cell responses evoked by single whisker stimulation in the corresponding and adjacent barrels showed that the whisker map has a pronounced topography at P5–7 (Armstrong-James 1975; Minlebaev et al. 2011). Moreover, spatially confined responses evoked by whisker stimulation using voltage-sensitive dye imaging and extracellular recordings suggested that the activity in the barrel cortex is already somatotopically organized at P0–1, prior to barrel formation (Yang et al. 2012). However, topographic precision regarding the whisker-related protomap in the prospective barrel cortex remains elusive. Here, using extracellular multiunit and patch-clamp recordings, we report that, in the neonatal P0–1 rat barrel cortex,

neurons are initially tuned to multiple whiskers and that the responses evoked by stimulation of the neighboring whiskers largely overlap. Segregation of the receptive fields occurs 2–3 days after birth, coinciding with the emergence of the anatomical barrel map. These results indicate that, during the critical period, the cortical whisker map undergoes a pivotal transition from an initially diffuse to a segregated stage and that its development involves competition between sensory inputs for their cortical target territories.

Materials and Methods

Surgery

All animal-use protocols followed the guidelines of the French National Institute of Health and Medical Research (INSERM, provisional approval N007.08.01) and the Kazan Federal University on the use of laboratory animals (ethical approval by the Institutional Animal Care and Use Committee of Kazan State Medical University N9-2013). Wistar rats of both sexes from postnatal days [P] 0–7 were used. P0 was the day of birth. The surgery was performed under isoflurane anesthesia (5% for induction and 1.5% during surgery). The skull of the animal was cleaned of skin and periosteum. Two plastic bars were fixed to the nasal and occipital bones of the rat's head by dental cement. The skull was covered with dental cement (Grip Cement) except for a 4- to 9-mm^2 window above the barrel cortex. Subsequently, animals were warmed and left for an hour to recover from anesthesia. During recordings, the head was fixed to the frame of the stereotaxic apparatus by the attached bars; animals were surrounded by a cotton nest and heated via a thermal pad (35°C–37°C). A chlorided silver wire, placed in the cerebellum or visual cortex, served as a ground electrode. Depending on the technique used, recordings were made from non-anesthetized or anesthetized by urethane (i/p injection; 0.5–1 g/kg) neonatal rats.

Stimulation

Before the experiment, whiskers were trimmed to a length of 4 mm. A needle (30G) was glued to the end of piezo benders (Noliac), and the tip of the whisker was inserted 2 mm into the blunt tip of the needle, so that the whisker rested snugly inside. To induce deflection of the piezo benders, square 40–70 V pulses of 10- or 25-ms duration were applied. To avoid depression of the evoked response, whiskers were alternately stimulated at 30-s intervals. Cortical responses to 50–100 stimuli were recorded for each whisker.

Recordings

Extracellular recordings of the local field potentials (LFPs) and multiple unit activity (MUA) were performed from the inner part of the dense cortical plate (CP; P0–3) or Layer 4 (in >P4 rats) (Fig. 1), either without anesthesia or under urethane anesthesia (0.5–1.5 g/kg). Urethane did not significantly modify the responses in this age group (Minlebaev et al. 2011), and therefore, the results obtained both with and without anesthesia were pooled. The skull was drilled to make the linear fissure above the barrel cortex (AP 0.3 to 1 mm; lateral 3–4 mm from bregma); "dura mater" was carefully dissected using a 30G needle. Recordings of LFP and MUA were performed using four-shank silicon probes (Neuronexus Technologies). The following types of electrode arrays were used: (1) 4 × 4 16-channel probes with a separation distance of 200 μm between shanks and a separation distance of 200 μm between electrodes in each shank; (2) 4 × 4 16-channel probes with 4 tetrodes horizontally separated by 200 μm; (3) 4 × 8 32-channel probes with a 200-μm separation distance between shanks and a 50-μm separation distance between electrodes in each shank, (5) 16-channel linear probes with 100-μm vertical separation distance. The signals from extracellular recordings were amplified and filtered (10 000×; 0.2 Hz–10 kHz) using a 32-channel amplifier (DIPSI, France or DigitalLynx, Neuralynx), digitized at 10 or 40 kHz (for single-unit recordings) and saved on a PC for post hoc analysis.

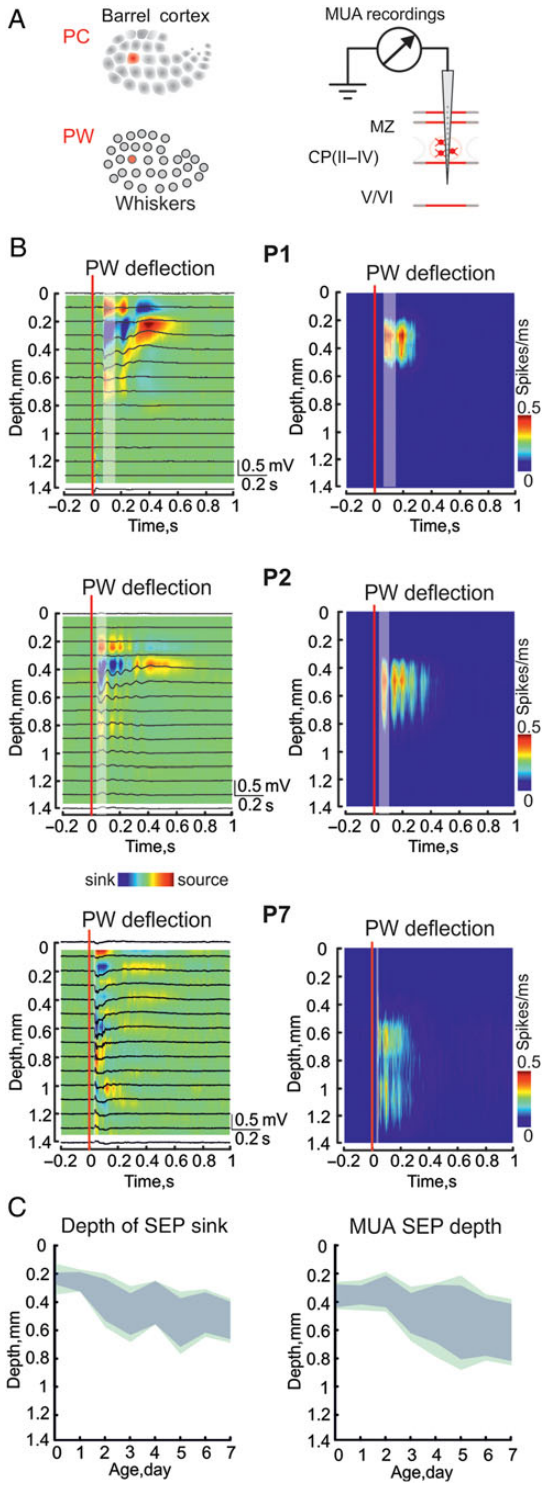

Figure 1. Developmental depth profile of the sensory-evoked responses. (*A*) Multisite extracellular recordings by linear 16-channel silicon probe of the MUA from CP (or L4) of single cortical site (PC, red) in barrel cortex evoked by stimulation of the corresponding principal whisker (PW, red). (*B*) Averaged evoked response (LFP, black lines) at different depths of the single cortical site overlaid on color-coded current source-density (CSD) analysis (left column) and PSTHs of MUA triggered by PW stimulations are shown for P0-, P2-, and P7-day-old animals (right column); red vertical line is PW stimulation; SEP is shown by shaded area. (*C*) Age-dependence of the depth of sensory-evoked responses calculated based on CSD (left) and MUA (right). Note that ranges of depths with short-latency LFP or MUA responses are shown by gray shading; Jackknife deviations are in light green shading.

Whole-cell recordings were performed under urethane anesthesia (0.5–1.5 g/kg). The skull and dura above the barrel cortex were removed, and the cortex was covered by low-gelling agarose (Sigma–Aldrich) to prevent drying and pulsations. Despite these precautions, we found patch-clamp recordings in P0–1 rats extremely difficult to perform, obtaining gigaseal and stable recordings with a success rate of <10%. The number of trials in each hole was also limited to 5, to avoid recordings from damaged tissue. It was thus difficult to obtain a complete receptive field, and the number of whiskers tested ranged from 2 to 13. Whole-cell recordings were performed using pipettes filled either with Cs-gluconate (130 Cs-gluconate, 13 CsCl, 0.1 $CaCl_2$, 1 ethylene glycol tetraacetic acid [EGTA], and 10 4-[2-hydroxyethyl]-1-piperazineethanesulfonic acid [HEPES], units are mM, pH 7.25) or K-gluconate (130 K-gluconate; 10 Na-gluconate; 4 NaCl; 4 Mg-ATP; 4 phosphocreatine; 10 HEPES [K]; 0.3 Na_2GTP, units are mM, pH 7.25) solutions. Glutamatergic excitatory postsynaptic currents (EPSCs) were recorded in voltage-clamp mode from the inner part of the CP or Layer 4 (in >P4 rats) cells at the reversal potential of the GABA(A) receptor-mediated currents (−70 mV). Whole-cell recordings were performed using an Axopatch 200B amplifier, digitized at 10 kHz with Digidata 1440 (Molecular Devices) and acquired on a PC using pClamp 10.2 software for post hoc analysis.

Data Analysis

Raw data were preprocessed using custom-written functions in MATLAB (MathWorks). Briefly, raw data were explored to detect MUA, following which the raw data were down-sampled to 1000 Hz. MUA was detected at a band-passed signal (>200 and <4000 Hz), where all negative events exceeding 3.5 SD were considered to be spikes (Fig. 2). Further analysis of extracellular units and whole-cell data was performed by custom-written, MATLAB-based programs and Chronux toolbox (Mitra and Pesaran 1999).

The whisker evoking maximal multiunit activity (MUA) response with the shortest latency was considered to be the principal whisker (PW). The thalamorecipient layer (inner part of dense cortical plate or Layer 4) was defined based on analysis of SEP, using current source density (CSD) analysis of (LFP) deflections during sensory-evoked potential (SEP) and analysis of MUA density (Fig. 1).

CSD was used to eliminate volume conduction and localize synaptic currents. CSD was computed for each recording site according to a differential scheme for the second derivative and smoothed with a triangular kernel of length 3 (Freeman and Nicholson 1975), so that current sinks were represented by negative values. Depth of SEP was calculated based on CSD analysis of the sensory-evoked LFP response, where (1) a sensory-evoked cortical signal was considered as SEP if the sink amplitude of the evoked response exceeded 20 SD of the sink amplitude distribution of the base line before stimulus and (2) the evoked cortical response had the shortest latency (Supplementary Fig. 1*A*). Depth of the thalamorecipient layer was also estimated based on presence of a burst of MUA with short latency; increased MUA was only considered a burst if it exceeded 5 SD of spontaneous MUA density (calculated from the 200-ms window before stimulus) (Supplementary Fig. 1*B*).

The evoked cortical response time was counted from whisker deflection to the onset of MUA, defined as the moment of maximal differ-

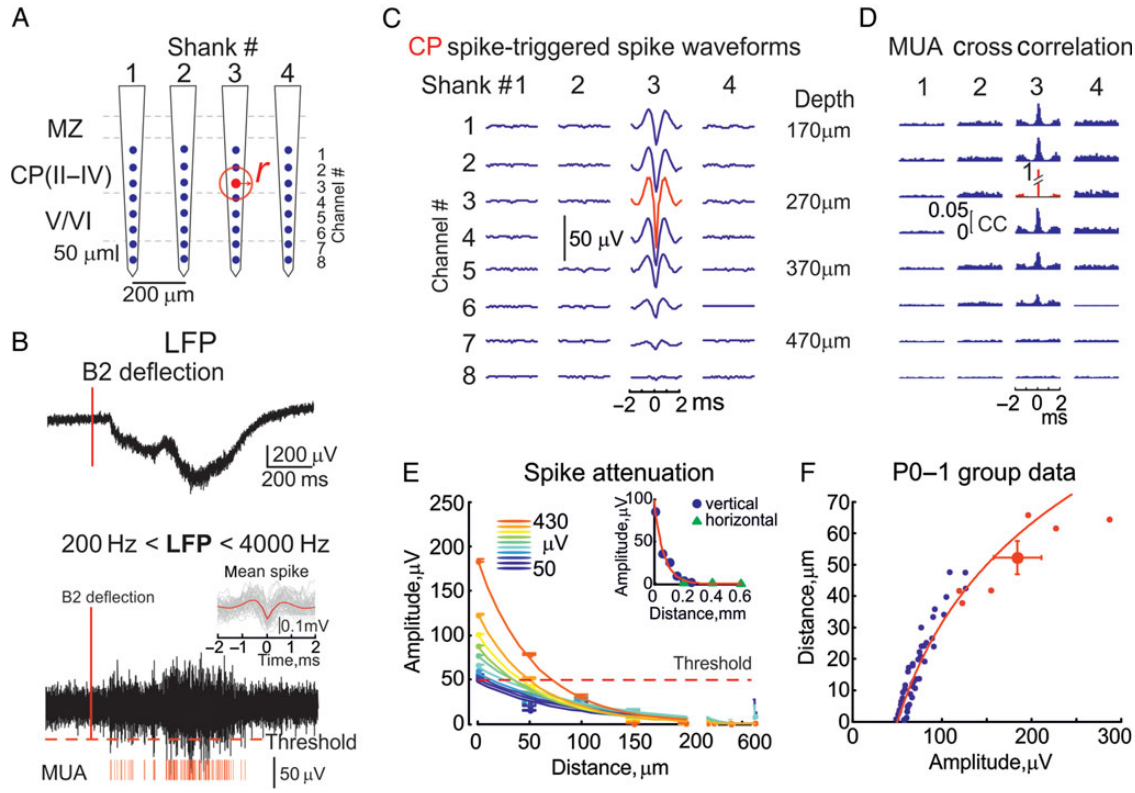

Figure 2. Estimation of distance of spike detection using extracellular recordings in neonatal rat neocortex. (*A*) Scheme of intracortical recordings using four-shank 4 × 8 32-channel electrode array from barrel cortex. Principal recording site at shank #3 and electrode #3 (red) is located in the inner part of the dense cortical plate (CP) and shows maximal short-latency response to a B2 whisker deflection. (*B*) Example of sensory response evoked at this electrode by B2 whisker deflection during wide-band recordings (0.2–10000 Hz) (top) and after band-passed filtering (200–4000 Hz, bottom). Red bars indicate spikes detected over threshold (49 µV) shown by horizontal dashed red line. Inset shows average spike (red) overlaid on 200 individual spikes (gray). (*C*) Local field potential averages at different recording sites triggered by spikes detected at the principal site (2316 spikes detected during 100 responses). (*D*) Cross-correlation of spikes detected at different recording sites versus spikes detected at the principal channel. (*E*) Dependence of the amplitude of LFP signals triggered by spikes sorted by amplitude into 10% bins and inset showing dependence of the amplitude of LFP signals triggered by all spikes detected at principal site on distance from principal site (as shown on panel C, taken both from vertical (blue circles) and horizontal (green triangle) neighbors). Dashed red lines indicate detection threshold. (*F*) Distance at which spikes attain threshold values (as shown on panel *E*) as a function of spike amplitude at principal site. Red circle indicates detection distance values for the largest group of spikes (118.8–286.6 µV). (*A–E*) recordings from 1 P0 rat; (*F*) pooled data from 6 P0–1 rats.

ence between the diagonal (which should correspond to the constant spike rate) and the cumulative sum of the peristimulus time histogram (PSTH) of the evoked MUA (Supplementary Fig. 2).

To characterize receptive and projection field (PF) sizes, first- and second-order adjacent whiskers were also stimulated, first-order adjacent whiskers (AWs1) being whiskers neighboring the PW and second-order adjacent whiskers (AWs2) being vibrissae two-away from the PW. Receptive fields in the barrel cortex were calculated as the total number of MUA in CP (or Layer 4) induced by alternate stimulation of the whiskers in a 1-s window after the stimulus, corrected for spontaneous MUA before whisker deflection. A similar procedure was used for whisker PF analysis, counting the total number of MUA induced by the PW in a 1-s window after stimulus on the electrode lying in CP (or Layer 4) on each shank.

Significances of the evoked cortical response parameters were tested using the nonparametric Wilcoxon test. The level of significance was set at $P < 0.05$. Variability of the estimates is shown as vertical bars of Jackknife deviation (Arvesen 1969).

To characterize the size of the cortical area where spikes are detected at a single recording site in the newborn rats, we analyzed spatial attenuation of spikes across the electrode array as shown in Figure 2 ($n = 6$ P0–1 rats). Local field potential averages triggered by spikes detected at a single "principal" recording site (shank #3, channel #3, red trace) showed a progressive spatial decrement in spike amplitudes, both vertically (along a shank, 50-μm site separation distance) and horizontally (between shanks, 200-μm shank separation distance) (Fig. 2*C*). The spatial decrement in spike amplitudes was also associated with decreased cross-correlation coefficients of spikes detected at distant sites (Fig. 2*D*). Dependence of the mean spike amplitude on the distance from the principal site could be fitted with an exponential function with a decay constant of 67.6 μm (Fig. 2*E* inset). We further sorted spikes detected on the principal site by 10% amplitude bins and found that, for all groups, spikes were attenuated with distance from the principal site (Fig. 2*E*). Spikes with larger amplitudes showed values exceeding spike detection thresholds (indicated by vertical red dashed line) at greater distances. Spikes within the largest spike amplitude bins (range from 119 to 287 μV; mean value of 184 ± 27 μV; $n = 6$ P0–1 rats) had threshold values at 52.2 ± 5.3 μm from the principal site (Fig. 2*A*). Assuming that the largest spikes are generated by neurons closest to the recording electrode, this value corresponds to the maximal radius of spike detection (r) in our experimental setting, as indicated by a red circle on Figure 2*F*, and it is close to the previously reported values (Cohen and Miles 2000; Henze et al. 2000).

Extraction of Single Units from MUA

Segments centered around the detected spikes on 1 recording site were extracted from all tetrode sites (Supplementary Fig. 3). For each channel, the waveforms of all spikes were pooled; first, 2 principal components of the waveform set were defined using principal component analysis. An 8-dimensional principal components vector was then created for each spike. Next, clusters corresponding to single-cell events were isolated by the clustering program KlustaKwik (http://klustakwik.sourceforge.net/) (Harris et al. 2002) (Fig. 5). Single-unit receptive fields were calculated based on the clusters that had: (1) units with clear refractory periods of <2 ms (Supplementary Fig. 3) and (2) units whose feature vectors followed a multivariate normal distribution (tested by calculation of the Mahalanobis distance of points from the cluster center [Gnanadesikan 1977; Johnson and Wichern 1992]) (Supplementary Fig. 3).

Results

Broad Receptive Fields in Neonatal Rat Barrel Cortex

To determine the initial functional state of the cortical barrel map, we explored the receptive fields of cortical neurons during extracellular recordings using multisite silicone probes in neonatal rat pups *in vivo* (postnatal days P0–1; P0 is day of birth; $n = 8$ rats; Fig. 3*A*). During the first 2 days after birth, a large number of whiskers evoked LFP responses organized in delta waves and spindle-burst oscillations associated with MUA at a single recording site in the prospective barrel cortex (Fig. 3*B–D*). MUA and the current sinks of these responses were maximal at the inner part of the CP at a depth of 200–400 μm from the cortical surface (Fig. 1*C*). The whisker evoking maximal MUA response with the shortest latency was considered to be the PW. To characterize the level of PW tuning, we compared the PW-evoked CP responses to the responses evoked by deflection of the surrounding primary and secondary adjacent whiskers (AW1 and AW2, respectively). Several comparisons indicated broad tuning to multiple whiskers at P0–1: (1) averages of AW1/PW and AW2/PW multiunit response ratios were 0.43 ± 0.05 and 0.23 ± 0.03, respectively (Fig. 3*D*); (2) overall, 8.7 ± 1.7 whiskers evoked significant ($P < 0.05$) MUA increase after their deflection (Supplementary Fig. 4); and (iii) on average, 4.8 ± 0.8 AWs evoked multiunit responses exceeding half of the PW-evoked responses (Fig. 3*E*).

Postnatal Segregation of Receptive Fields

Broad tuning to multiple whiskers was only observed during the first 2 days after birth. Starting from P2–3, clearly segregated adult-like receptive fields emerged (Simons 1978; Armstrong-James and Fox 1987; Roy et al. 2011), characterized by: (1) a reduction in the AW1/PW and AW2/PW multiunit response ratios, to 0.17 ± 0.01 and 0.1 ± 0.02, respectively (Fig. 3*D*), with a preferential tuning to the neighboring whiskers within rows rather than to arcs (Armstrong-James et al. 1992; Roy et al. 2011) (Fig. 4, see also Supplementary Fig. 5), (2) a reduction in the total number of whiskers evoking significant multiunit response, to 6.4 ± 0.5 whiskers (Supplementary Fig. 4) (Carvell and Simons 1988; Moore and Nelson 1998; Zhu and Connors 1999; Borgdorff et al. 2007; Roy et al. 2011), and (iii) almost total elimination of the AWs (0.3 ± 0.1) evoking more than half of the PW-evoked multiunit response ($n = 21$; P2–7 rats; Fig. 3*E*, see also Supplementary Fig. 4*B* for 20% bin size). Single units recorded using tetrodes showed similar refinement of the receptive fields during the postnatal period (Fig. 5). At P0–1, the PW-evoked responses (1.5 ± 0.3 spikes/response) did not significantly differ from the AW1-evoked responses (0.7 ± 0.2 spikes/response; $n = 6$ single units from 2 P0–1 rats; $P > 0.05$, Fig. 5*E*). In P4–5 rat pups, the PW-evoked responses (1.9 ± 0.9 spikes/response) became significantly stronger than the AW1-evoked responses (0.37 ± 0.1 spikes/response; $n = 10$ single units from 2 P4–5 rats; $P < 0.001$). Thus, receptive fields in the barrel cortex show a developmental transition from initially diffuse organization at birth, characterized by broad tuning of cortical neurons to multiple whiskers, to a segregated stage emerging 2–3 days after birth, where neurons become preferentially tuned to a single PW.

Postnatal Segregation of Whisker Projection Fields in Barrel Cortex

Activation of cortical neurons by multiple whiskers implies that sensory input from a single whisker activates larger cortical territories in newborn rats. To test this hypothesis, the responses evoked by single whisker stimulation were recorded using multishank electrodes with 200-μm horizontal separation distance (Fig. 6*A*). We first analyzed the receptive fields for each shank as described earlier (Fig. 6*B*, bottom plots) and

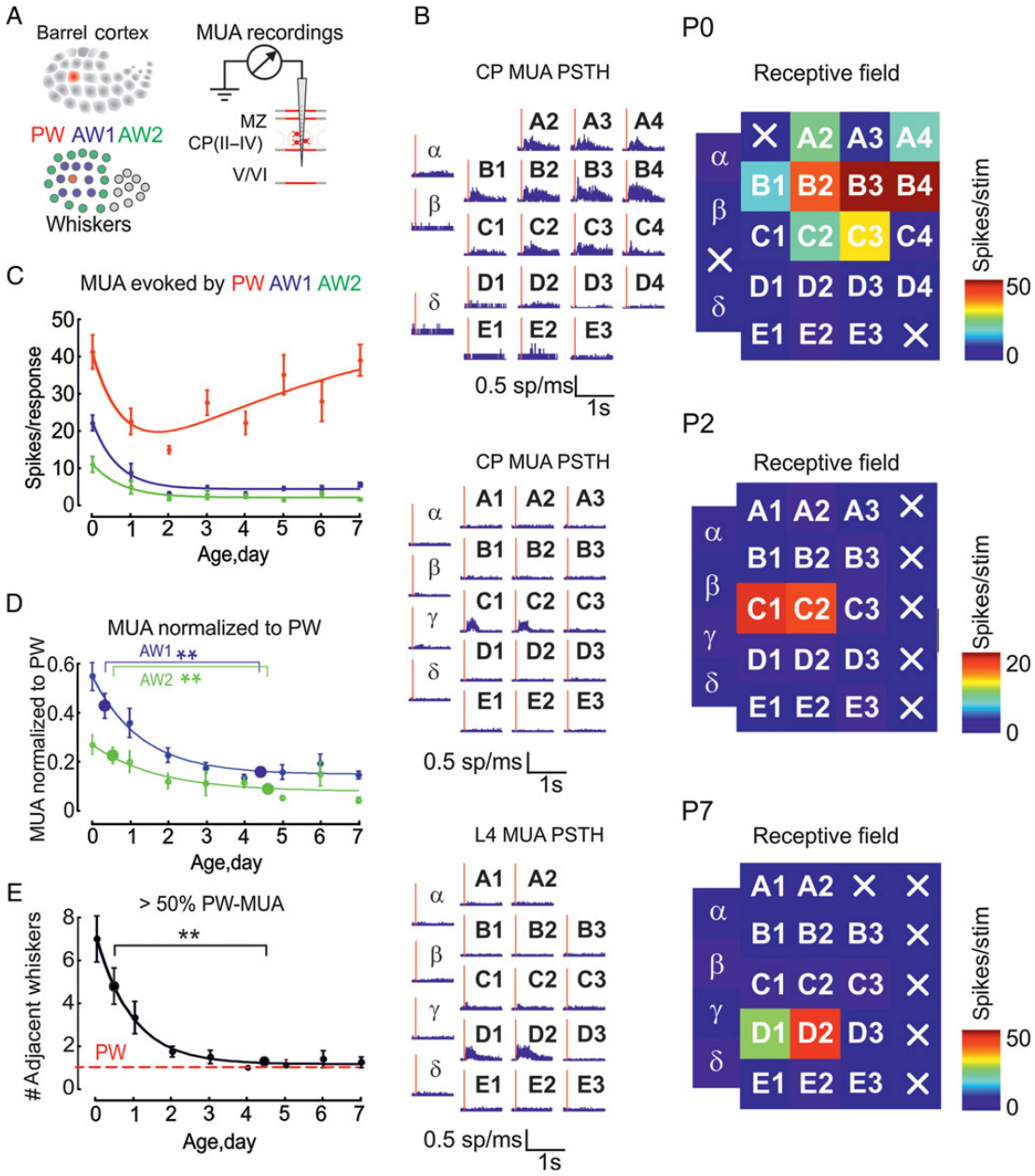

Figure 3. Postnatal development of receptive fields in barrel cortex. (*A*) Multisite extracellular recordings of cortical responses evoked by stimulation of the principal whisker (PW, red); adjacent whiskers of the 1st (AW1, blue) and 2nd order (AW2, green). (*B*) Multiunit peristimulus time histograms (PSTHs, left column) and MUA density-based, color-coded receptive fields (right column) at postnatal days P0, P2, and P7. Each cell of the whisker matrix contains the value of a single whisker-evoked integral multiunit response, except for non-tested whiskers marked by X. Age-dependence of the multiunit responses evoked by the stimulation of PW, AW1, and AW2 (*C*) and multiunit AW1/PW and AW2/PW response ratios (*D*). Data are fitted using exponential decay function. (*E*) Age-dependence of the number of adjacent whiskers inducing a cortical multiunit response exceeding half of the PW-evoked response. (*C–E*) pooled data from 29 rats. $^{**}P < 0.01$.

then compared the responses evoked by single whisker stimulation at different shanks (Fig. 6*B*, top traces). In P0–1 rats, multiunit responses evoked by single whisker stimulation were observed at multiple cortical sites (Fig. 6*B*). The cortical PF of a single whisker, estimated as a distance at which half-maximal response (PF50) is observed (Fig. 6*C*), was 240 ± 22 μm in P0–1 rats ($n = 8$). With maturation, the whisker PF shrank to 159 ± 6 μm at P2–7 (Fig. 6*F,G,H*; $n = 21$). Thus, in agreement with broad tuning of cortical neurons at a single cortical site to multiple whiskers, inputs from individual whiskers also show broad cortical PFs during the early postnatal period. Moreover, similar developmental profiles are observed for both the projection (Fig. 6*H*) and receptive (Fig. 3*C–E*) fields.

Developmental Segregation of Synaptic Inputs

To explore the synaptic mechanisms underlying the generation of diffuse responses in newborn rats, we performed whole-cell recordings from the cortical neurons of the dense cortical plate (Fig. 7*C*). At P0–1, PW stimulation evoked barrages of EPSCs (Fig. 7*C*). Total charge transfer during synaptic PW-evoked responses was −5.9 ± 3.6 pC at a holding potential of −70 mV

($n = 6$; Fig. 7*B*). In agreement with the results of extracellular recordings, stimulation of adjacent whiskers in P0–1 rats revealed broad receptive fields for the excitatory synaptic responses, with an integral AW1-evoked response of -1.4 ± 0.6 pC ($34 \pm 10\%$ of the PW-evoked response; $n = 6$). In older animals, the latency of the PW-evoked synaptic responses shortened to 49 ± 3 ms whereas the integral PW-evoked synaptic response increased to -17.1 ± 2.3 pC, AW1-evoked responses were -2.2 ± 0.6 pC ($n = 13$ cells; P4–7 rats, Fig. 7*B*). Thus, the synaptic receptive fields of a single cortical neuron also showed a transition from a diffuse state at P0–1, characterized by robust excitatory synaptic responses evoked in a single neuron by multiple whiskers, to a segregated stage, characterized by predominance of the responses evoked by PW over AWs.

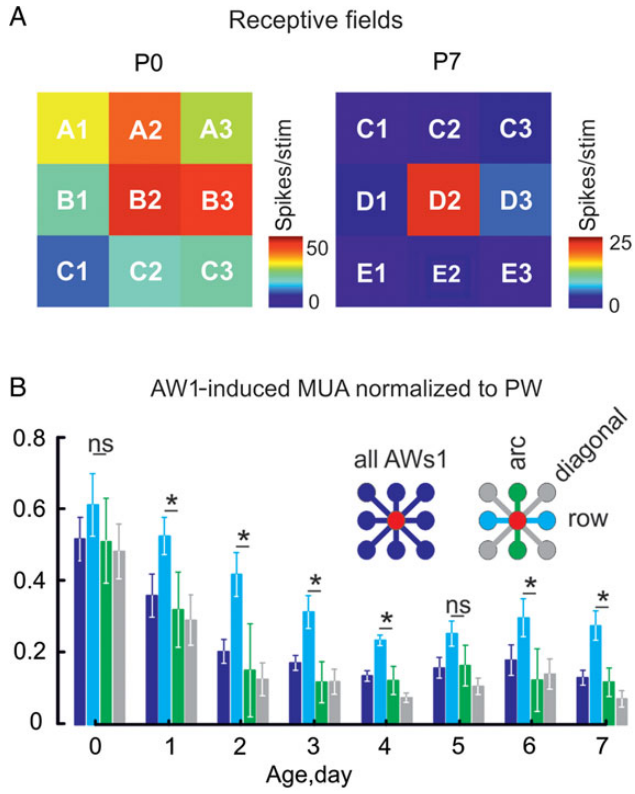

Figure 4. Population receptive fields for adjacent whiskers in rows and arcs. (*A*) MUA density-based, color-coded receptive fields for PW and its AWs1 at postnatal days P0 and P7. (*B*) Age-dependence of the multiunit AW1/PW response ratios for all AWs1 (dark blue), AWs in rows (light blue), in arcs (green) and at diagonals (gray). Note an emerging bias toward AWs in rows starting from P1.

Discussion

The main findings of the present study are the following: (1) cortical neurons in the neonatal rat barrel cortex are strongly activated by a large number of whiskers; accordingly, whisker PFs are also broad and largely overlap during the first 2 postnatal days, and (2) segregation of the receptive and PFs in the barrel cortex occurs by P2–3, coinciding with formation of anatomical barrels.

Our results indicate that the receptive fields in the rat barrel cortex are imprecise at birth. The blurriness of the early receptive fields may reflect coarse and overlapping connectivity in the thalamus and cortex. While in rats the barrelettes pattern in the brainstem appears to have already developed by P0 (Chiaia et al. 1992; Waite et al. 2000), patterning in the VPM occurs during the first postnatal days (Belford and Killackey 1979). However, pruning of over-numerous lemniscal inputs to thalamic neurons was shown in studies in mice (Arsenault and Zhang 2006; Zhang et al. 2013). In rats, thalamic afferents reach the cortical plate at birth (Erzurumlu and Jhaveri 1990; Rhoades et al. 1990; Catalano et al. 1996; Molnar et al. 2003). Although, in both rats and mice, the topological precision of thalamo-cortical projection at birth is under debate (Senft and

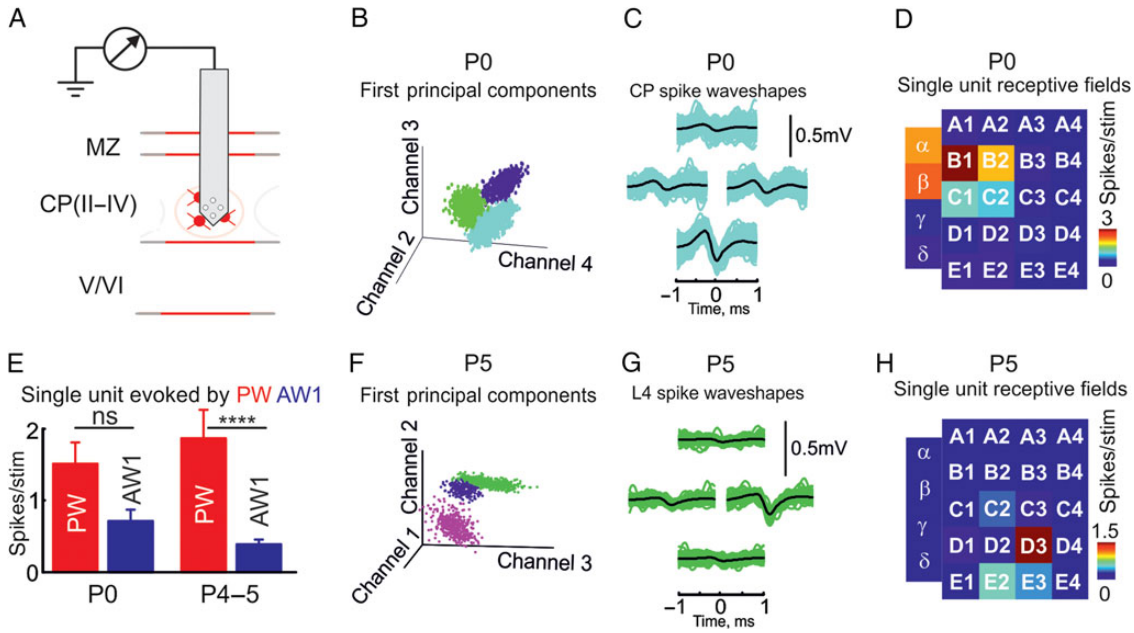

Figure 5. Postnatal development of single-unit receptive fields. (*A*) Recordings of MUA from CP (or L4) using 4 microelectrodes in tetrode configuration. (*B*,*F*) Clusters of single units grouped by close principal component values. (*C*,*G*) Spike waveshapes of the single units belonging to 1 cluster. (*D*,*H*) Color-coded receptive fields for the single-unit clusters shown in C and G; (*E*) averaged single-unit response evoked by stimulation of PW and AW1 for age groups P0 ($n = 6$ clusters) and P4–5 ($n = 10$ clusters).

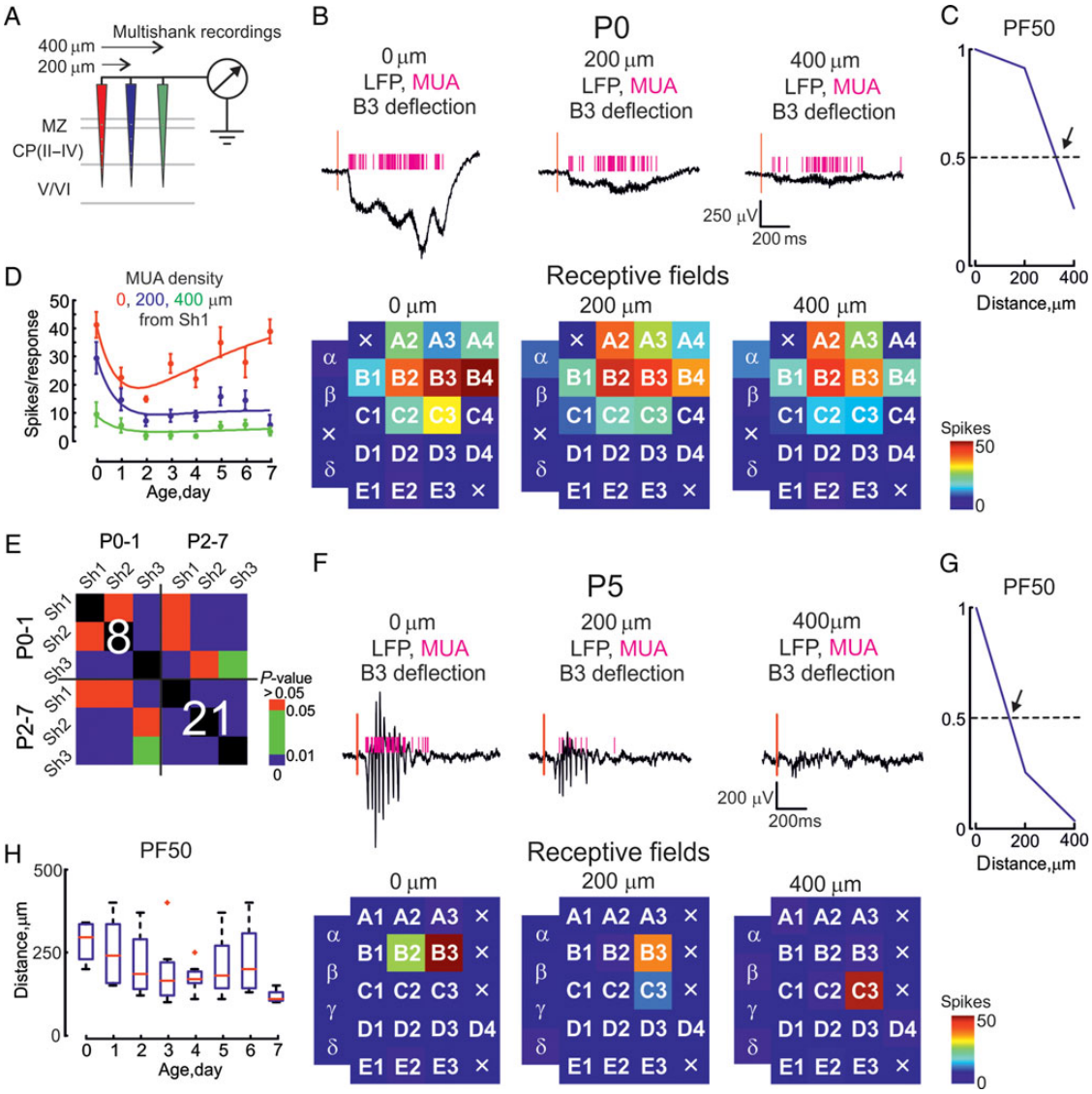

Figure 6. Postnatal segregation of whisker cortical PFs. (*A*) Scheme of recordings using multishank multisite extracellular electrodes (200-µm horizontal separation distance). Multishank recordings of responses evoked by PW stimulation for the principal (0 µm) and adjacent (200 and 400 µm) cortical sites in dense cortical plate in P0 (*B*) and in Gr layer of P5 (*F*) rat pups; receptive fields for each cortical site are shown under the traces; (*C,G*) cortical PFs for these experiments; arrows indicate that the normalized MUA density crossed the 50% threshold level used to estimate the size of a single whisker cortical PF (PF50); (*D*) age-dependence of the multiunit responses evoked by a single whisker for the principal and adjacent cortical sites. Data are fitted using exponential decay function; (*E*) *P*-value map of the MUA density evoked by PW stimulations recorded by principal shank and other shanks in 2 rat pup age groups (P0–1 and P2–7). Note that within each age group, *P*-values were obtained from paired data comparisons. The numbers on the diagonal indicate the number of animals within each group. (*H*) Age-dependence of a single whisker PF50 distance, where medians of boxplots are shown by red lines. (*D,H*) Pooled data from 29 rats.

Woolsey 1991; Agmon et al. 1995; Catalano et al. 1996; Rebsam et al. 2002; Lee et al. 2005), the initial pattern of thalamic axons does not show barrel-like organization (Erzurumlu and Jhaveri 1990; Jhaveri et al. 1991). By P2, thalamic axons start to organize in barrel-like patches, and by P4, an adult-like barrel pattern emerges in which thalamo-cortical axons organize into barrel-shaped bundles with a topographic projection of thalamic barreloids to cortical barrels (Erzurumlu and Jhaveri 1990; Rhoades et al. 1990; Agmon et al. 1995). At the postsynaptic level, cytoarchitectonic barrel formation and differentiation of Layer 4 from the cortical plate start at around P3 in both cats and rats (Rice et al. 1985; Blue et al. 1991; Jhaveri et al. 1991). In early postnatal development, Layer 4 cells of the barrel cortex do not show dendritic orientation; throughout the first postnatal week, they gradually orient their dendrites toward, and position themselves around, the TCA terminal patches corresponding to whiskers. This involves NMDA-R-dependent pruning of the branches extending to neighboring barrels (Espinosa et al. 2009). In addition, feedforward inhibition, which sets a temporal window of integration of thalamic inputs and contributes to surround inhibition, is absent during the first postnatal days (Daw et al. 2007; Minlebaev et al. 2011). Finally, a large number of pure NMDA-R-based silent thalamo-cortical synapses (Feldman et al. 1999; Hanse et al. 2013), in conjunction with the high affinity of NMDA-Rs to glutamate (Patneau and Mayer 1990) and a large extracellular space (Thomas et al. 2011), may lead to a spillover and paracrine actions of glutamate released from thalamic axons and growth

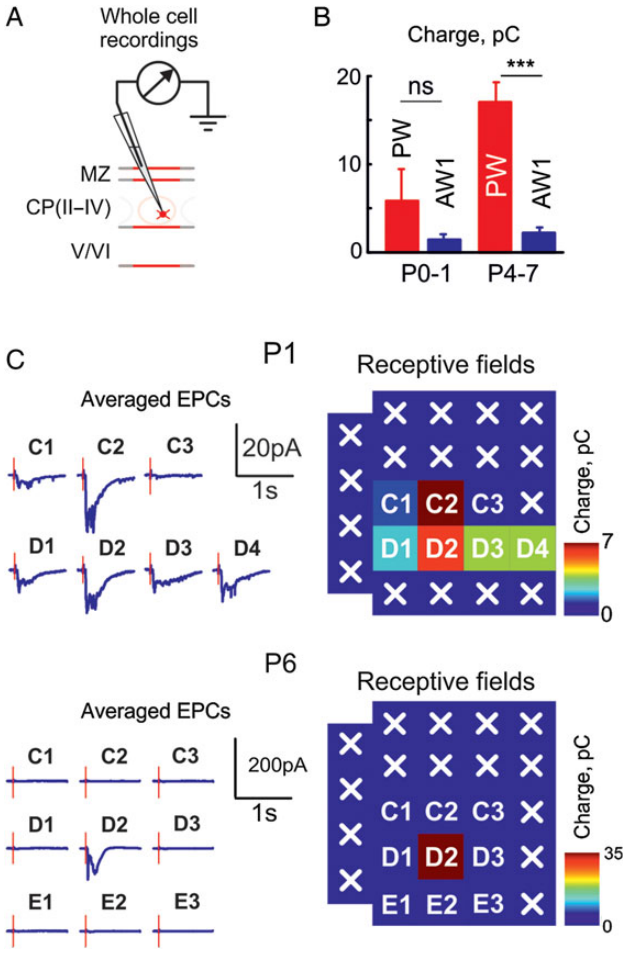

Figure 7. Synaptic basis for diffuse receptive fields in neonatal rats. (*A*) Whole-cell recordings of responses evoked by deflection of PW and AW1; (*B*) averaged charge transfer (left) and AWs1/PW charge transfer ratio (right) for the age groups P0–1 ($n = 6$ cells) and P4–7 ($n = 13$); (*C*) averaged evoked whole-cell responses (−70 mV holding potential, left) and corresponding color-coded receptive fields based on the excitatory postsynaptic charge transfer in P1 and P6 rat pups. MZ, marginal zone; V/VI, Layers 5/6.

cones at distant sites (Kullmann and Asztely 1998). All of the above anatomical and functional properties are subject to rapid developmental changes, and these may contribute to a segregation of the receptive fields during postnatal development.

Despite the fact that the initial thalamo-cortical synapses are limited in number and weak and that their vast majority are pure NMDA-R-based "silent" at the resting membrane potential (Feldman et al. 1999; Hanse et al. 2013), sensory inputs evoked robust excitatory postsynaptic currents, LFP and multiunit cortical responses at birth, and multiunit responses showed a developmental decline over a period from P0 to P2–3 (Fig. 3*C*). Generation of such robust responses at birth likely involves powerful temporal summation of slow NMDA and kainate receptor-mediated currents at the immature thalamo-cortical synapses (Kidd and Isaac 1999; Minlebaev et al. 2007; Minlebaev et al. 2009), which should elicit extensive depolarization in the immature neurons, with very high (in the gigaohms range) membrane resistance (LoTurco et al. 1991; Zhou and Hablitz 1996; Mienville and Pesold 1999). Another factor contributing to robust responses at birth is the above-mentioned lack of feedforward inhibition and the large (indefinite in cells lacking GABAergic inputs) temporal window for integration of excitatory inputs (Daw et al. 2007; Minlebaev et al. 2011).

Our results support the hypothesis that sensory map development involves initial formation of the basic protomap via innate mechanisms, followed by its activity-dependent refinement (Katz and Shatz 1996; Rakic et al. 2009; Erzurumlu and Gaspar 2012). This paradigm has been observed in a number of developing sensory circuits, including the optic tectum (Ruthazer et al. 2003), the visual (Chen and Regehr 2000), and somatosensory thalamus (Arsenault and Zhang 2006; Zhang et al. 2013), and the superior colliculus (Brown et al. 2000), as well as during development of neuromuscular connections (Sanes and Lichtman 1999; Lichtman and Colman 2000) and climbing fiber synapses in the cerebellum (Kano and Hashimoto 2009). In contrast, ocular dominance columns in the visual cortex (Crowley and Katz 2002), odor maps in the olfactory bulb (Lin et al. 2000; Zheng et al. 2000), and cortical interlaminar synapses in the somatosensory cortex (Bureau et al. 2004) have been shown to develop with considerable specificity from the start. Here, we found a certain level of precision already in the innate protomap, with 1 whisker evoking maximal response at the cortical site within the prospective barrel cortex and with a gradual decrease in the responses evoked by adjacent whiskers of the first and second order. Somatotopic organization of activity at birth has also been reported in a study by Yang and colleagues, using a combination of voltage-sensitive dye imaging and extracellular recordings (Yang et al. 2012). The authors concluded that innate protomaps are precise, although the level of protomap precision was not evaluated in that study. Our findings suggest a model in which the barrel map develops neither from a "tabula rasa" nor a precise protomap but, from a state with a sub-columnar level of precision, created via innate mechanisms ensuring crude topography. Further refinement of map precision to columnar level occurs during the first 2–3 postnatal days, and this process is characterized by competitive interactions between whiskers. We propose that the robust and overlapping whisker-evoked responses described in the present study are instrumental to such refinement. Once somatotopic correspondence is established by P2–3, topographic thalamo-cortical synapses may further mature through a potentiation supported by topographic EGOs (Minlebaev et al. 2011).

Supplementary Material

Supplementary material can be found at: http://www.cercor.oxfordjournals.org/.

Funding

Financial support from ANR (grant ANR-09-MNPS-006 to RK), the Government of the Russian Federation (grant 11.G34.31.0075 and the program of competitive growth of Kazan University to RK and grant RFBR 13-04-01237a to MM), and FRM (DEQ20110421301 to RK) is acknowledged.

Notes

We thank D. Zaynutdinova for help with the histology, and Drs. A. Sirota, M. Colonnese, I. Bureau, and R. Cossart for their valuable comments on the manuscript. *Conflict of Interest*: None declared.

References

Agmon A, Yang LT, Jones EG, O'Dowd DK. 1995. Topological precision in the thalamic projection to neonatal mouse barrel cortex. J Neurosci. 15:549–561.

Armstrong-James M. 1975. The functional status and columnar organization of single cells responding to cutaneous stimulation in neonatal rat somatosensory cortex S1. J Physiol. 246:501–538.

Armstrong-James M, Fox K. 1987. Spatiotemporal convergence and divergence in the rat S1 "barrel" cortex. J Comp Neurol. 263:265–281.

Armstrong-James M, Fox K, Das-Gupta A. 1992. Flow of excitation within rat barrel cortex on striking a single vibrissa. J Neurophysiol. 68:1345–1358.

Arsenault D, Zhang ZW. 2006. Developmental remodelling of the lemniscal synapse in the ventral basal thalamus of the mouse. J Physiol. 573:121–132.

Arvesen. 1969. Jackknifing U-statistics. Ann Math Stat. 40:2076–2100.

Belford GR, Killackey HP. 1979. The development of vibrissae representation in subcortical trigeminal centers of the neonatal rat. J Comp Neurol. 188:63–74.

Blue ME, Erzurumlu RS, Jhaveri S. 1991. A comparison of pattern formation by thalamocortical and serotonergic afferents in the rat barrel field cortex. Cereb Cortex. 1:380–389.

Borgdorff AJ, Poulet JF, Petersen CC. 2007. Facilitating sensory responses in developing mouse somatosensory barrel cortex. J Neurophysiol. 97:2992–3003.

Brecht M, Sakmann B. 2002. Dynamic representation of whisker deflection by synaptic potentials in spiny stellate and pyramidal cells in the barrels and septa of layer 4 rat somatosensory cortex. J Physiol. 543:49–70.

Brown A, Yates PA, Burrola P, Ortuno D, Vaidya A, Jessell TM, Pfaff SL, O'Leary DDM, Lemke G. 2000. Topographic mapping from the retina to the midbrain is controlled by relative but not absolute levels of EphA receptor signaling. Cell. 102:77–88.

Bureau I, Shepherd GM, Svoboda K. 2004. Precise development of functional and anatomical columns in the neocortex. Neuron. 42:789–801.

Carvell GE, Simons DJ. 1988. Membrane potential changes in rat SmI cortical neurons evoked by controlled stimulation of mystacial vibrissae. Brain Res. 448:186–191.

Catalano SM, Robertson RT, Killackey HP. 1996. Individual axon morphology and thalamocortical topography in developing rat somatosensory cortex. J Comp Neurol. 367:36–53.

Chen C, Regehr WG. 2000. Developmental remodeling of the retinogeniculate synapse. Neuron. 28:955–966.

Chiaia NL, Bennett-Clarke CA, Eck M, White FA, Crissman RS, Rhoades RW. 1992. Evidence for prenatal competition among the central arbors of trigeminal primary afferent neurons. J Neurosci. 12:62–76.

Cohen I, Miles R. 2000. Contributions of intrinsic and synaptic activities to the generation of neuronal discharges in in vitro hippocampus. J Physiol. 524:485–502.

Colonnese MT, Kaminska A, Minlebaev M, Milh M, Bloem B, Lescure S, Moriette G, Chiron C, Ben-Ari Y, Khazipov R. 2010. A conserved switch in sensory processing prepares developing neocortex for vision. Neuron. 67:480–498.

Crowley JC, Katz LC. 2002. Ocular dominance development revisited. Curr Opin Neurobiol. 12:104–109.

Daw MI, Ashby MC, Isaac JT. 2007. Coordinated developmental recruitment of latent fast spiking interneurons in layer IV barrel cortex. Nat Neurosci. 10:453–461.

Erzurumlu RS, Gaspar P. 2012. Development and critical period plasticity of the barrel cortex. Eur J Neurosci. 35:1540–1553.

Erzurumlu RS, Jhaveri S. 1990. Thalamic axons confer a blueprint of the sensory periphery onto the developing rat somatosensory cortex. Brain Res Dev Brain Res. 56:229–234.

Espinosa JS, Wheeler DG, Tsien RW, Luo L. 2009. Uncoupling dendrite growth and patterning: single-cell knockout analysis of NMDA receptor 2B. Neuron. 62:205–217.

Feldman DE. 2009. Synaptic mechanisms for plasticity in neocortex. Annu Rev Neurosci. 32:33–55.

Feldman DE, Brecht M. 2005. Map plasticity in somatosensory cortex. Science. 310:810–815.

Feldman DE, Nicoll RA, Malenka RC. 1999. Synaptic plasticity at thalamocortical synapses in developing rat somatosensory cortex: LTP, LTD, and silent synapses. J Neurobiol. 41:92–101.

Feldmeyer D, Brecht M, Helmchen F, Petersen CC, Poulet JF, Staiger JF, Luhmann HJ, Schwarz C. 2013. Barrel cortex function. Prog Neurobiol. 103:3–27.

Fox K. 2008. Barrel cortex. Cambridge (UK): Cambridge University Press.

Freeman JA, Nicholson C. 1975. Experimental optimization of current source-density technique for anuran cerebellum. J Neurophysiol. 38:369–382.

Gnanadesikan R. 1977. Methods for statistical data analysis of multivariate observations. New-York: Wiley.

Hanse E, Seth H, Riebe I. 2013. AMPA-silent synapses in brain development and pathology. Nat Rev Neurosci. 14:839–850.

Harris KD, Henze DA, Hirase H, Leinekugel X, Dragoi G, Czurko A, Buzsaki G. 2002. Spike train dynamics predicts theta-related phase precession in hippocampal pyramidal cells. Nature. 417:738–741.

Henze DA, Borhegyi Z, Csicsvari J, Mamiya A, Harris KD, Buzsaki G. 2000. Intracellular features predicted by extracellular recordings in the hippocampus in vivo. J Neurophysiol. 84:390–400.

Jhaveri S, Erzurumlu RS, Crossin K. 1991. Barrel construction in rodent neocortex: role of thalamic afferents versus extracellular matrix molecules. Proc Natl Acad Sci USA. 88:4489–4493.

Johnson RA, Wichern DA. 1992. Applied Multivariate Statistical Analysis. Englewood Cliffs, NJ: Prentice Hall.

Kano M, Hashimoto K. 2009. Synapse elimination in the central nervous system. Curr Opin Neurobiol. 19:154–161.

Katz LC, Shatz CJ. 1996. Synaptic activity and the construction of cortical circuits. Science. 274:1133–1138.

Khazipov R, Colonnese M, Minlebaev M. 2013. Neonatal cortical rhythms. In: Rubenstein Rakic P, editors. Neural Circuits Development and Function in the Healthy and Diseased Brain: Comprehensive Developmental Neuroscience. San-Diego (CA): Elsevier. p 131–154.

Kidd FL, Isaac JT. 1999. Developmental and activity-dependent regulation of kainate receptors at thalamocortical synapses. Nature. 400:569–573.

Kullmann DM, Asztely F. 1998. Extrasynaptic glutamate spillover in the hippocampus: evidence and implications. Trends Neurosci. 21:8–14.

Lee LJ, Iwasato T, Itohara S, Erzurumlu RS. 2005. Exuberant thalamocortical axon arborization in cortex-specific NMDAR1 knockout mice. J Compar Neurol. 485:280–292.

Lichtman JW, Colman H. 2000. Synapse elimination and indelible memory. Neuron. 25:269–278.

Lin DM, Wang F, Lowe G, Gold GH, Axel R, Ngai J, Brunet L. 2000. Formation of precise connections in the olfactory bulb occurs in the absence of odorant-evoked neuronal activity. Neuron. 26:69–80.

Lopez-Bendito G, Lujan R, Shigemoto R, Ganter P, Paulsen O, Molnar Z. 2003. Blockade of GABA(B) receptors alters the tangential migration of cortical neurons. Cereb Cortex. 13:932–942.

LoTurco JJ, Blanton MG, Kriegstein AR. 1991. Initial expression and endogenous activation of NMDA channels in early neocortical development. J Neurosci. 11:792–799.

McCandlish CA, Li CX, Waters RS. 1993. Early development of the SI cortical barrel field representation in neonatal rats follows a lateral-to-medial gradient: an electrophysiological study. Exp Brain Res. 92:369–374.

Mienville JM, Pesold C. 1999. Low resting potential and postnatal upregulation of NMDA receptors may cause Cajal-Retzius cell death. J Neurosci. 19:1636–1646.

Minlebaev M, Ben-Ari Y, Khazipov R. 2007. Network mechanisms of spindle-burst oscillations in the neonatal rat barrel cortex in vivo. J Neurophysiol. 97:692–700.

Minlebaev M, Ben Ari Y, Khazipov R. 2009. NMDA receptors pattern early activity in the developing barrel cortex In Vivo. Cereb Cortex. 19:688–696.

Minlebaev M, Colonnese M, Tsintsadze T, Sirota A, Khazipov R. 2011. Early gamma oscillations synchronize developing thalamus and cortex. Science. 334:226–229.

Mitra PP, Pesaran B. 1999. Analysis of dynamic brain imaging data. Biophys J. 76:691–708.
Mohns EJ, Blumberg MS. 2010. Neocortical activation of the hippocampus during sleep in infant rats. J Neurosci. 30:3438–3449.
Molnar Z, Kurotani T, Higashi S, Yamamoto N, Toyama K. 2003. Development of functional thalamocortical synapses studied with current source-density analysis in whole forebrain slices in the rat. Brain Res Bull. 60:355–371.
Moore CI, Nelson SB. 1998. Spatio-temporal subthreshold receptive fields in the vibrissa representation of rat primary somatosensory cortex. J Neurophysiol. 80:2882–2892.
O'Leary DD, Sahara S. 2008. Genetic regulation of arealization of the neocortex. Curr Opinion Neurobiol. 18:90–100.
Patneau DK, Mayer ML. 1990. Structure-activity relationships for amino acid transmitter candidates acting at N-methyl-D-aspartate and quisqualate receptors. J Neurosci. 10:2385–2399.
Petersen C. 2007. The functional organization of the barrel cortex. Neuron. 56:339–355.
Rakic P. 1976. Prenatal genesis of connections subserving ocular dominance in the rhesus monkey. Nature. 261:467–471.
Rakic P, Ayoub AE, Breunig JJ, Dominguez MH. 2009. Decision by division: making cortical maps. Trends Neurosci. 32:291–301.
Rebsam A, Seif I, Gaspar P. 2002. Refinement of thalamocortical arbors and emergence of barrel domains in the primary somatosensory cortex: a study of normal and monoamine oxidase a knock-out mice. J Neurosci. 22:8541–8552.
Rhoades RW, nett-Clarke CA, Chiaia NL, White FA, Macdonald GJ, Haring JH, Jacquin MF. 1990. Development and lesion induced reorganization of the cortical representation of the rat's body surface as revealed by immunocytochemistry for serotonin. J Comp Neurol. 293:190–207.
Rice FL, Gomez C, Barstow C, Burnet A, Sands P. 1985. A comparative analysis of the development of the primary somatosensory cortex: interspecies similarities during barrel and laminar development. J Comp Neurol. 236:477–495.
Roy NC, Bessaih T, Contreras D. 2011. Comprehensive mapping of whisker-evoked responses reveals broad, sharply tuned thalamocortical input to layer 4 of barrel cortex. J Neurophysiol. 105:2421–2437.
Ruthazer ES, Akerman CJ, Cline HT. 2003. Control of axon branch dynamics by correlated activity in vivo. Science. 301:66–70.
Sanes JR, Lichtman JW. 1999. Development of the vertebrate neuromuscular junction. Annu Rev Neurosci. 22:389–442.
Senft SL, Woolsey TA. 1991. Growth of thalamic afferents into mouse barrel cortex. Cereb Cortex. 1:308–335.
Simons DJ. 1978. Response properties of vibrissa units in rat SI somatosensory neocortex. J Neurophysiol. 41:798–820.
Thomas CG, Tian H, Diamond JS. 2011. The relative roles of diffusion and uptake in clearing synaptically released glutamate change during early postnatal development. J Neurosci. 31:4743–4754.
Tolner EA, Sheikh A, Yukin AY, Kaila K, Kanold PO. 2012. Subplate neurons promote spindle bursts and thalamocortical patterning in the neonatal rat somatosensory cortex. J Neurosci. 32:692–702.
Waite PM, Ho SM, Henderson TA. 2000. Afferent ingrowth and onset of activity in the rat trigeminal nucleus. Eur J Neurosci. 12:2781–2792.
Woolsey TA, Van der Loos H. 1970. The structural organization of layer IV in the somatosensory region (SI) of mouse cerebral cortex. The description of a cortical field composed of discrete cytoarchitectonic units. Brain Res. 17:205–242.
Yang JW, An S, Sun JJ, Reyes-Puerta V, Kindler J, Berger T, Kilb W, Luhmann HJ. 2012. Thalamic network oscillations synchronize ontogenetic columns in the newborn rat barrel cortex. Cereb Cortex. 23:1299–1316.
Yang JW, Hanganu-Opatz IL, Sun JJ, Luhmann HJ. 2009. Three patterns of oscillatory activity differentially synchronize developing neocortical networks *in vivo*. J Neurosci. 29:9011–9025.
Zhang ZW, Peterson M, Liu H. 2013. Essential role of postsynaptic NMDA receptors in developmental refinement of excitatory synapses. Proc Natl Acad Sci USA. 110:1095–1100.
Zheng C, Feinstein P, Bozza T, Rodriguez I, Mombaerts P. 2000. Peripheral olfactory projections are differentially affected in mice deficient in a cyclic nucleotide-gated channel subunit. Neuron. 26:81–91.
Zhou FM, Hablitz JJ. 1996. Postnatal development of membrane properties of layer I neurons in rat neocortex. J Neurosci. 16:1131–1139.
Zhu JJ, Connors BW. 1999. Intrinsic firing patterns and whisker-evoked synaptic responses of neurons in the rat barrel cortex. J Neurophysiol. 81:1171–1183.